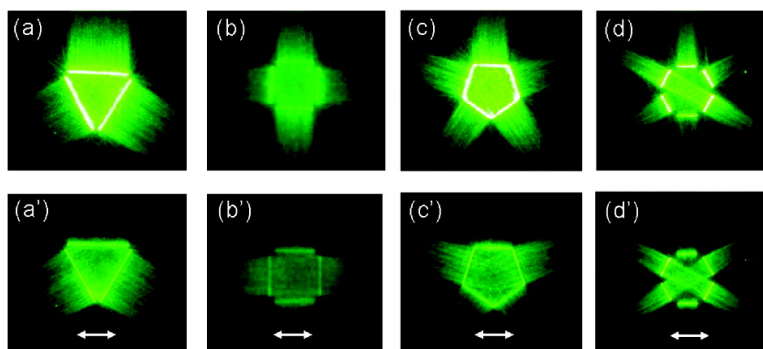


Broad Band Two-Dimensional Manipulation of Surface Plasmons

Zhaowei Liu, Yuan Wang, Jie Yao, Hyesog Lee, Werayut Srituravanich, and Xiang Zhang

Nano Lett., **2009**, 9 (1), 462-466 • DOI: 10.1021/nl803460g • Publication Date (Web): 19 December 2008

Downloaded from <http://pubs.acs.org> on January 15, 2009



More About This Article

Additional resources and features associated with this article are available within the HTML version:

- Supporting Information
- Access to high resolution figures
- Links to articles and content related to this article
- Copyright permission to reproduce figures and/or text from this article

[View the Full Text HTML](#)



ACS Publications
High quality. High impact.

Broad Band Two-Dimensional Manipulation of Surface Plasmons

Zhaowei Liu,^{†‡} Yuan Wang,[‡] Jie Yao,[‡] Hyesog Lee,[‡] Werayut Srituravanich,[‡] and Xiang Zhang^{*,‡,§}

NSF Nanoscale Science and Engineering Center (NSEC), 5130 Etcheverry Hall, University of California, Berkeley, California, 94720, and Materials Sciences Division, Lawrence Berkeley National Laboratory, 1 Cyclotron Road, Berkeley, California 94720

Received November 14, 2008; Revised Manuscript Received December 10, 2008

ABSTRACT

A plasmonic interference pattern can be formed when multiple surface plasmon waves overlap coherently. Utilizing a sharp edge coupling mechanism, we experimentally demonstrate plasmonic interference patterns that can be designed at will by shaping the edges in a metallic film. The patterns can also be dynamically tailored by adjusting the wavelength, the polarization, and the incident angle of the excitation light beam. Possessing the subdiffraction limited feature resolution, this dynamical manipulation method of surface plasmon patterns will have profound potentials in nanolithography, particle manipulation, and other related fields.

Surface plasmon polaritons (SPPs) are surface electromagnetic waves formed by collective oscillation of electrons at a metal/dielectric interface.¹ The fundamental SPP properties have been extensively studied in 1970s and widely applied thereafter in a number of important applications such as surface plasmon resonance sensing^{2,3} and imaging,^{4,5} surface-enhanced Raman scattering,^{6,7} surface-enhanced second harmonic generation,⁸⁻¹⁰ etc. The recent advancement in nanoscale fabrication techniques has given rise to even more fascinating applications in superimaging beyond the diffraction limit,¹¹⁻¹⁴ subwavelength electromagnetic wave guiding,¹⁵⁻¹⁸ plasmonic lithography,¹⁹⁻²³ plasmonic ruler,^{24,25} optical negative refraction,²⁶ as well as cancer treatment by metallic nanoparticles,^{27,28} which has remarkably extended and transformed the horizon of the field of plasmonics.

A light beam in three-dimensional (3D) free space can be converted into a two dimensionally (2D) confined SPP wave as long as the momentum mismatch between them is compensated by a coupling element. The sacrifice of dimensionality, however, results in extraordinary "optical frequency but X-ray wavelength" property, i.e., an SPP wavelength much smaller than that of the excitation light, as well as strong electromagnetic field enhancement in the SPP near-field. As a straightforward consequence, converting free space light into SPPs on a planar surface should lead to devices or applications that possess higher spatial resolution and higher near-field energy density. Hence a precise yet

flexible design of surface structures on a metallic film to couple the free space light into various SPPs and to guide their propagation is on demand. In this paper, we present a general scheme to manipulate SPP interference patterns by designing the surface structure shape and controlling the wavelength, incidence angle, and polarization of the excitation light beam. We demonstrate lithographic pattern formation and fluorescence imaging to exemplify the strength of this design.

The dispersion relation for the SPP at an interface between semi-infinite metal and dielectric materials is expressed as¹

$$k_{sp} = \sqrt{\frac{\epsilon_1 \epsilon_m}{\epsilon_1 + \epsilon_m} \frac{2\pi}{\lambda_0}} \quad (1)$$

where k_{sp} is the SPP wave vector, λ_0 is the light wavelength in vacuum, and ϵ_1 and ϵ_m are the permittivities of the dielectric and metal, respectively. A typical SPP dispersion curve based on the above equation is illustrated in Figure 1a. Since the wave vector of the SPP is always larger than that of the light in the surrounding media at the same frequency (i.e., smaller wavelength of SPPs), a momentum compensation coupling mechanism is necessary to excite the SPPs. A grating is considered as one of the best SPP couplers because it can provide an additional discrete wave vector in a very efficient way. A single sharp edge (or a slit) can also be used to excite SPPs, where the light diffracted from the corner gains very broad band wave vectors; the interface will automatically select the components with matched wave vector with SPPs and support their propagation,^{29,30} (see also Figure 1b). While the nonresonant nature of this process will reduce the coupling efficiency, these simple structures will drastically reduce the complexity of sample fabrication. In

* Corresponding author, xiang@berkeley.edu.

[†] Current address: Electrical & Computer Engineering, University of California, San Diego, 9500 Gilman Dr, La Jolla, CA 92093.

[‡] University of California, Berkeley.

[§] Lawrence Berkeley National Laboratory.

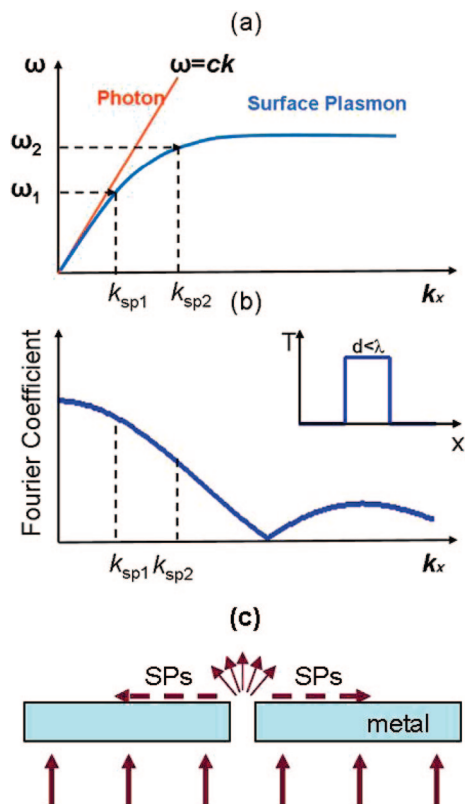


Figure 1. (a) A typical dispersion curve for surface plasmons. To excite surface plasmons by an incident light beam at a specific frequency, the momentum mismatch between them has to be compensated. (b) Fourier spectrum of a rectangular function with subwavelength width. It represents the possible wave vectors of the light gained by diffraction over a slit shown in the inset. (c) A schematic to show the surface plasmon excitation by a slit in metallic film.

the rest of our paper, we will focus on how to utilize the shape of either a slit or single edge to control the SPP interference patterns on a metallic surface.

We would like to start with a simplest situation—SPP interference between two antipropagating SPP waves. As an example, the simulated total electrical field distribution at the cross section of an infinitely long aluminum strip is shown in Figure 2a under a normally incident excitation light at 365 nm from the bottom. The refractive indices for substrate and the photoresist are 1.52 and 1.6, respectively. The aluminum film thickness is 100 nm, which is enough to block direct transmission of the incident light so that all of the fields on top of the aluminum film are purely from SPPs. The width of the aluminum stripe is $2\ \mu\text{m}$, which is around the SPP propagation length. Clearly, both the edges of the aluminum film act as a line source of SPPs. SPPs propagate away from the edges and form a uniform interference pattern in the middle. Instead of the commonly used silver and gold in other plasmonic applications at visible light, aluminum is selected in this specific case due to its relatively less loss at UV frequency.

Two samples were used in our experiment to demonstrate the SPP interference by means of photolithography. The first sample, schematically shown in Figure 2b, comprises a

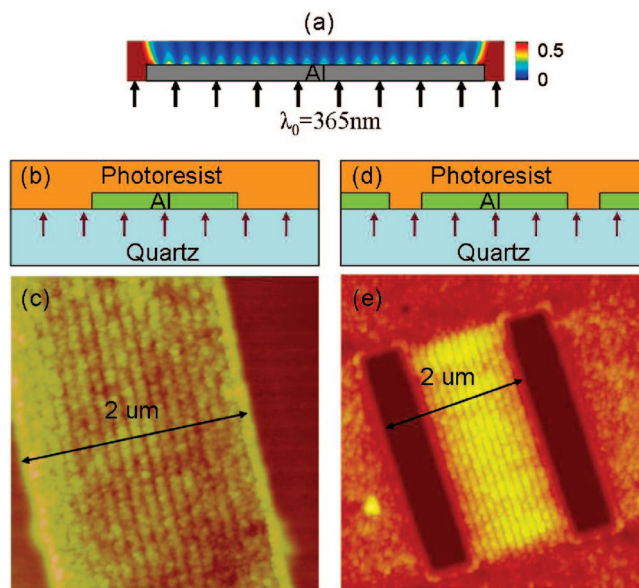


Figure 2. (a) Numerical simulation shows SPP interference pattern on top of an Al strip. (b, d) Schematic experimental configurations of two samples fabricated by e-beam lithography and lift-off process and focus ion beam milling, respectively. (c, e) AFM image of the exposure pattern using samples (b) and (d), respectively. The aluminum thickness is 100 nm in all cases.

$2\ \mu\text{m}$ wide aluminum strip on quartz substrate. It was fabricated by e-beam lithography followed by a lift-off process. This sample utilizes a sharp aluminum edge to excite SPPs. The second sample, schematically shown in Figure 2d, was obtained by focused ion beam (FIB, FEI Strata 201 XP) milling (slit openings are about 700 nm wide) in an aluminum film deposited on the quartz wafer. The SPPs will be excited by the slit in this sample. The aluminum thickness is 100 nm in both cases. Subsequently, a 15 nm thick OmniCoat (MicroChem, refractive index is 1.57) layer was spun on both samples to increase the adhesion between aluminum and exposed photoresist. Finally, a negative near-UV photoresist (SU-8) was spun on the top of the OmniCoat. Both samples were exposed with an exposure dose of $200\ \text{mJ}/\text{cm}^2$ by a filtered mercury lamp with a radiation peak at 365 nm. After the development, the topography of the recorded features was measured by an atomic force microscope (AFM, Dimension 3100, Veeco).

The exposure results for both samples are presented in panels c and e of Figure 2, respectively. Clearly, one-dimensional gratings which come from the SPP interference were obtained between the slits/edges in both samples with good contrast and uniformity. In the second sample (Figure 2e), SPP also propagates outward from the slits without experience of interference, which can be clearly told on the aluminum film outside of the double slits region, although the contrast is lower compared to the center part. The grating periodicities in both cases are about 120 nm, which agree well with the simulation results. Considering the free space working wavelength is 365 nm, the SPP interference pattern line width has reached a 60 nm line width which is equivalent to $\lambda/6$. We should point out that both of the sample preparations can also be completely done by conventional

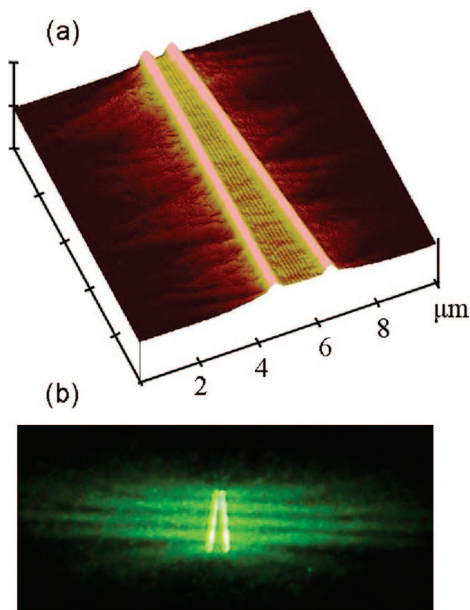


Figure 3. (a) AFM image of an exposure pattern with two unparallel slits in a 100 nm aluminum film. The slit width is around 200 nm. (b) Fluorescent image observed by optical microscopy shows the SPP interference pattern outside of the two unparallel slits in a 200 nm thick silver film.

photolithography since the required feature size of the structure in metal film is in micrometer scale.

As we discussed in our previous simulation study,²⁰ the contrast of the interference pattern will not be affected by the distance between the edges which is not much larger than the SPP propagation length. We repeat the previous experiment with two unparallel slits (the slit width is around 300 nm and the angle between the slits is about 6°). As shown in Figure 3a, the contrast of the interference pattern is virtually constant at locations with different slit spaces. The pattern in the center of the slits remains unchanged and new fringes emerge from the periphery which is also consistent with the simulation. This result also indicates that the SPP reflection from a single slit is negligible so that no cavity effect needs to be considered.

We also developed a method to deduce the wavelength of a SPP wave by a simple far field measurement of the fringe period outside of the slit pair shown in Figure 3a. The fringe pattern is formed by SPP waves outside of the slit pair. The fringe period strongly relates with the tilt angle between the slits and can be much larger than the SPP wavelength, so it is quite easy to be observed under conventional optical microscopy by coating a layer of PMMA with fluorescent dyes,³⁰ as shown in Figure 3b. Notice the structure in Figure 3b is made by silver, which is different than that made with aluminum in the case of Figure 3a. The illumination light is 532 nm and the fluorescent dye is Rhodamine 6G. The fringe period is about 3 μm, so that the SPP wavelength can be deduced as ~310 nm by knowing the angle between the slits is 12°.

Since SPPs are essentially two dimensionally confined on a metal–dielectric interface, their interference patterns can be controlled by arranging different 2D geometries of the

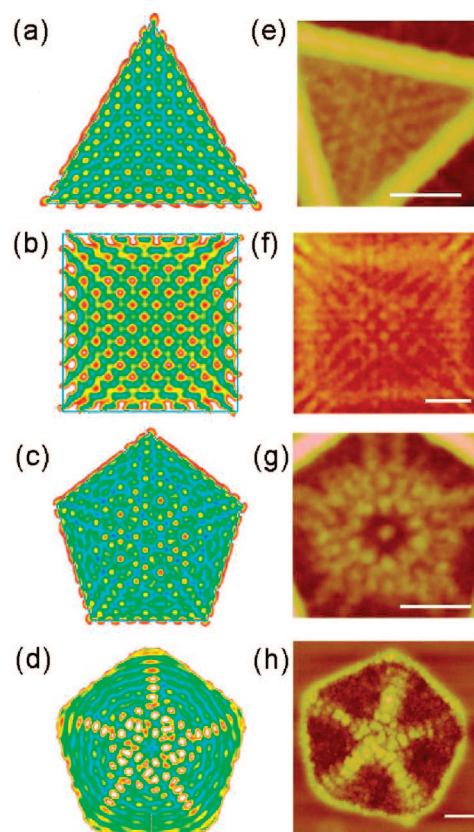


Figure 4. Simulation a–d and experimental results e–h using a 100 nm thick aluminum plate with various edge/slit shapes: (a, e) triangle; (b, f) square; (c, g) pentagon; (d, h) pentagon with rounded corners. The side lengths are 2, 2, 1.5, and 1.5 μm, respectively in (a–d). The excitation light had angular polarization in all the simulations. The scale bars in all of the AFM images represent 500 nm. The side lengths of the triangle, square, pentagon, and rounded pentagon structures used in the experiment are 2, 2.5, 2, and 1.6 μm, respectively.

slits/edges. Figure 4a–d show simulated SPP interference patterns with four geometries. Obviously, not only periodic but also quasi-periodic and even more complicated 2D patterns can be realized. The lithography experimental results (see Figure 4e–h) clearly show the formation of different interference patterns predicted by simulations. A single collimated *i*-line beam from a mercury lamp ($\lambda = 365$ nm) is used to generate all these patterns with exposure time typically less than 10 s, corresponding to a dose of around 18 mJ/cm². Compared with the pattern formation by free laser beam interference, one obvious advantage of SPP interference is the higher resolution as we discussed above. In addition, SPP interference requires a much simpler setup. To achieve a complex laser interference pattern, multiple laser beams have to be very precisely directed and controlled by complicated optics. As for SPP interference in our case, all of the complicated optics can simply be replaced by slits/edges with well-designed shapes and only one excitation beam is required.

For a structure with fixed shape, the interference pattern can still be dynamically adjusted by the polarization and incident angle of the excitation light beam. The SPPs can only be efficiently excited when the incident light has a

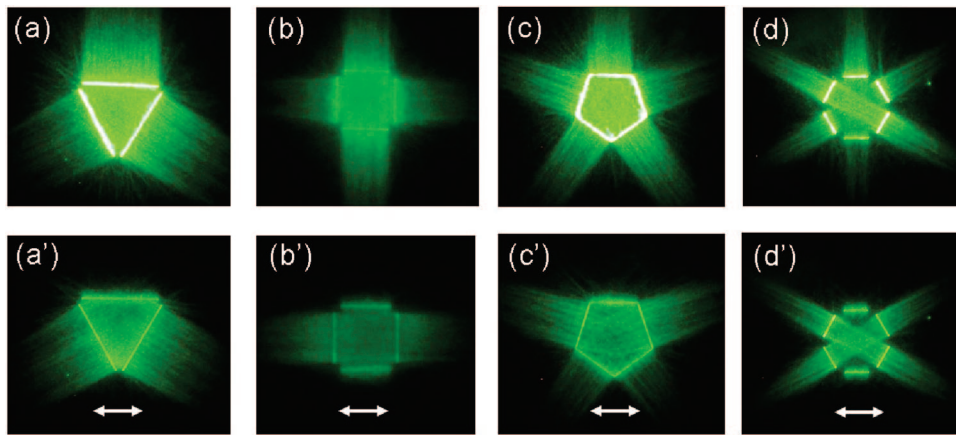


Figure 5. Fluorescent images observed by optical microscopy under normal incident nonpolarized illumination (a–d) and horizontally polarized illumination (a'–d').

polarization perpendicular to the slit.²⁹ Therefore, the strength of the SPPs at different portions of the slit can be arbitrarily tuned by adjusting the polarization of the excitation light beam. For example, in Figure 5 the fluorescent images illustrate how the SPPs propagate along the surface for different geometries. The excitation light beam is normally illuminated to the structure. Nonpolarized light and horizontally polarized light were used in Figure 5, panels a–d and a'–d', respectively. Clearly, all the slits can be treated as SPP sources and get equally excited under nonpolarized light illumination. In the middle of the triangular, square, pentagonal, and hexagonal structure, three, four, five, and six SPP beams form interference patterns, respectively (the interference patterns are not distinguishable by the far field fluorescent imaging method). After a polarizer is added in the excitation beam, as indicated by the white arrows, the SPP sources at the horizontal slits are completely turned “off”. The interference patterns inside of the triangle, square, pentagon, and hexagon are then formed by two, two, four, and four SPP beams, respectively.

When the excitation beam is normal to the structure, the SPP propagation direction is always perpendicular to the slit as shown above. If an in-plane wavevector is introduced by an inclined illumination light beam, the SPP propagation direction can be adjusted (as schematically shown in Figure 6a). This method has been used to tune the focus position of a plasmonic lens³⁰ and now can also be utilized to further improve the tunability of the SPP interference patterns on the surface. Figure 6b–d shows a few examples by combining the polarization and incident angle control. A more complicated dynamic pattern is also possible by rotating the polarization direction and controlling the incident angle at different parts of the slit.

Only one beam is used in all of our previous experiments, which has shown the simplicity of our SPP interference method for applications such as nanolithography. One could also notice that each SPP source (slit/edge) can be addressed individually by parallel multiple focusing techniques.^{31,32} Given all the aforementioned flexibilities, the SPP interference can be used as a platform to form various desired dynamic patterns with fine resolution. The rule of thumb to

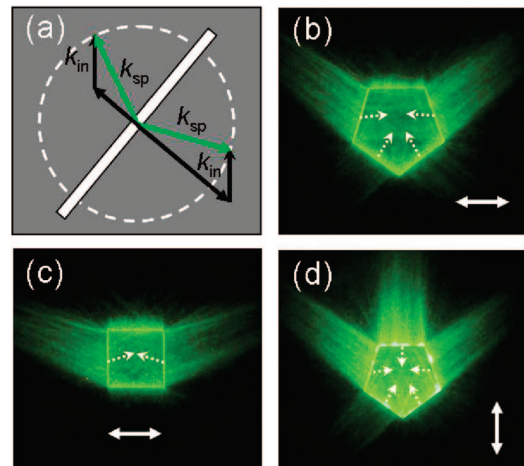


Figure 6. (a) Wavevector conservation sketch to show the propagation direction of the SPP waves excited by an angled incident illumination beam. (b–d) Fluorescent images observed by optical microscopy under angled incident illumination with different polarizations. The double-headed white arrows represent the polarization direction. The dotted white arrows represent the surface plasmon propagation directions excited from each side.

form such patterns is as follows. First, the SPP sources are positioned by arranging multiple slits around the working area. The number of slits is the maximum beams needed in the interference, and the length of the slit provides the divergence for the SPP beam from each slit. Second, control the SPP beam direction by incident angle of the excitation light. The SPP beam from each slit has full access to be addressed individually. Third, the intensity of each SPP source can also be individually controlled by the polarization direction of the excitation light. It is worth emphasizing that all these principles can be equivalently operated at various working frequencies which is important for potential applications. For instance, SPPs with multicolors can be manipulated independently on the same structure for more complex pattern control. The selection of the metals depends on the relative loss at the working frequencies. Generally, silver is the best at visible frequency, while aluminum is a better choice in the UV to deep UV regions.

In conclusion, we presented an experimental study of SPP interference patterns on a two-dimensional surface. By

converting free space light into smaller wavelength SPPs, the SPP interference patterns possess subwavelength resolution with respect to free space light beam. We successfully demonstrated the high SPP interference lithography resolution ($\lambda/6$) with a feature size of ~ 60 nm. By using an edge/slit excitation mechanism, 2D complex interference patterns have been obtained with different edge/slit geometries. In addition, the patterns can also be manipulated by adjusting incident beam angle, polarization direction, and light frequency.

Acknowledgment. This work was supported by the U.S. Department of Energy under Contract No. DE-AC02-05CH11231, and partially supported by the Center for Scalable and Integrated Nanomanufacturing (SINAM), an NSF Nanoscale Science and Engineering Center (NSEC), under award number DMI-0327077.

References

- (1) Raether, H. *Surface Plasmons on Smooth and Rough Surfaces and on Gratings*; Springer: Heidelberg, 1988.
- (2) Nylander, C.; Liedberg, B.; Lind, T. *Sens. Actuators* **1982**, *3*, 79–88.
- (3) Homola, J.; Yee, S. S.; Gauglitz, G. *Sens. Actuators B* **1999**, *54*, 3–15.
- (4) Hickel, W.; Kamp, D.; Knoll, W. *Nature* **1989**, *339*, 186–186.
- (5) Brockman, J. M.; Nelson, B. P.; Corn, R. M. *Annu. Rev. Phys. Chem.* **2000**, *51*, 41–63.
- (6) Kneipp, K.; Wang, Y.; Kneipp, H.; Perelman, L. T.; Itzkan, I.; Dasari, R. R.; Feld, M. S. *Phys. Rev. Lett.* **1997**, *78*, 1667–1670.
- (7) Nie, S. M.; Emery, S. R. *Science* **1997**, *275*, 1102–1104.
- (8) Wokaun, A.; Bergman, J. G.; Heritage, J. P.; Glass, A. M.; Liao, P. F.; Olson, D. H. *Phys. Rev. B* **1981**, *24*, 849–856.
- (9) Chen, C. K.; de Castro, A. R. B.; Shen, Y. R. *Phys. Rev. Lett.* **1981**, *46*, 145–148.
- (10) Kim, E. M.; Elovikov, S. S.; Murzina, T. V.; Nikulin, A. A.; Aktsipetrov, O. A.; Bader, M. A.; Marowsky, G. *Phys. Rev. Lett.* **2005**, *95*, 227402.
- (11) Fang, N.; Lee, H.; Sun, C.; Zhang, X. *Science* **2005**, *308*, 534–537.
- (12) Melville, D. O. S.; Blaikie, R. J. *Opt. Express* **2005**, *13*, 2127–2134.
- (13) Liu, Z. W.; Lee, H.; Xiong, Y.; Sun, C.; Zhang, X. *Science* **2007**, *315*, 1686–1686.
- (14) Liu, Z. W.; Durant, S.; Lee, H.; Pikus, Y.; Fang, N.; Xiong, Y.; Sun, C.; Zhang, X. *Nano Lett.* **2007**, *7*, 403–408.
- (15) Zia, R.; Selker, M. D.; Brongersma, M. L. *Phys. Rev. B* **2005**, *71*, 165431.
- (16) Barnes, W. L.; Dereux, A.; Ebbesen, T. W. *Nature* **2003**, *424*, 824–830.
- (17) Pile, D. P. F.; Gramotnev, D. K. *Opt. Lett.* **2004**, *29*, 1069–1071.
- (18) Bozhevolnyi, S. I.; Volkov, V. S.; Devaux, E.; Laluet, J. Y.; Ebbesen, T. W. *Nature* **2006**, *440*, 508–511.
- (19) Srituravanich, W.; Fang, N.; Sun, C.; Luo, Q.; Zhang, X. *Nano Lett.* **2004**, *4*, 1085–1088.
- (20) Liu, Z. W.; Wei, Q. H.; Zhang, X. *Nano Lett.* **2005**, *5*, 957–961.
- (21) Shao, D. B.; Chen, S. C. *Appl. Phys. Lett.* **2004**, *86*, 253107.
- (22) Luo, X. G.; Ishihara, T. *Appl. Phys. Lett.* **2004**, *84*, 7480–7482.
- (23) Wang, L.; Uppuluri, S. M.; Jin, E. X.; Xu, X. F. *Nano Lett.* **2006**, *6*, 361–364.
- (24) Su, K. H.; Wei, Q. H.; Zhang, X.; Mock, J. J.; Smith, D. R.; Schultz, S. *Nano Lett.* **2003**, *3*, 1087–1090.
- (25) Sönnichsen, C.; Reinhard, B. M.; Liphardt, J.; Alivisatos, A. P. *Nat. Biotechnol.* **2005**, *23*, 741–745.
- (26) Yao, J.; Liu, Z.; Liu, Y.; Wang, Y.; Sun, C.; Bartal, G.; Stacy, A.; Zhang, X. *Science* **2008**, *321*, 930.
- (27) O’Neal, D. P.; Hirsch, L. R.; Halas, N. J.; Payne, J. D.; West, J. L. *Cancer Lett.* **2004**, *109*, 181–176.
- (28) Loo, C.; Lowery, A.; Halas, N.; West, J.; Drezek, R. *Nano Lett.* **2005**, *5*, 709–711.
- (29) Liu, Z. W.; Steele, J. M.; Srituravanich, W.; Pikus, Y.; Sun, C.; Zhang, X. *Nano Lett.* **2005**, *5*, 1726–1729.
- (30) Liu, Z. W.; Steele, J. M.; Lee, H.; Zhang, X. *Appl. Phys. Lett.* **2006**, *88*, 171108.
- (31) Fujita, K.; Nakanura, O.; Kaneko, T.; Oyamada, M.; Takamatsu, T.; Kawata, S. *Opt. Commun.* **2000**, *174*, 7–12.
- (32) Wang, S.; Szobota, S.; Wang, Y.; Volgraf, M.; Liu, Z. W.; Sun, C.; Trauner, D.; Isacoff, E. Y.; Zhang, X. *Nano Lett.* **2007**, *7*, 3859.

NL803460G